Numerically exact long-time magnetization dynamics at the nonequilibrium Kondo crossover of the Anderson impurity model

Guy Cohen, Emanuel Gull, David R. Reichman, Andrew J. Millis, and Eran Rabani

Phys. Rev. B **87**, 195108 — Published 8 May 2013

DOI: 10.1103/PhysRevB.87.195108

Numerically Exact Long Time Magnetization Dynamics at the Nonequilibrium Kondo Crossover of the Anderson Impurity Model

Guy Cohen,[1,2] Emanuel Gull,[3,4] David R. Reichman,[1] Andrew J. Millis,[2] and Eran Rabani[5]

[1]*Department of Chemistry, Columbia University, New York, New York 10027, U.S.A.*
[2]*Department of Physics, Columbia University, New York, New York 10027, U.S.A.*
[3]*Max Planck Institut für Physik komplexer Systeme, Dresden, Germany*
[4]*Department of Physics, University of Michigan, Ann Arbor, MI 48109, U.S.A.*
[5]*School of Chemistry, The Sackler Faculty of Exact Sciences, Tel Aviv University, Tel Aviv 69978, Israel*

We investigate the dynamical and steady-state spin response of the nonequilibrium Anderson model to magnetic fields, bias voltage, and temperature using a numerically exact method combining a bold-line quantum Monte Carlo technique with the memory function formalism. We obtain converged results in a range of previously inaccessible regimes, in particular the spin dynamics for a range of temperatures down to the crossover to the Kondo domain. We provide predictions for novel nonequilibrium phenomena, including non-monotonic temperature dependence of observables at high bias voltage and oscillatory quench dynamics at high magnetic fields.

Strongly correlated open quantum systems appear in a wide variety of physical situations, including quantum dots in semiconductor heterostructures[1,2], molecular electronics[3,4] and the dynamics of cold atoms[5]. These systems consist of a finite, interacting region coupled to a continuous set of non-interacting "bath" or "lead" states which may be maintained at differing thermodynamic states. It is natural to describe open systems in terms of quantum impurity models, which have been used in the description of magnetic impurities in metals[6], the adsorption of atoms on a surface[7] and as auxiliary problems in the dynamical mean field approximation to extended lattice systems[8]. More recently, they have also been of interest in the nonequilibrium context of mesoscopic transport[9,10] and nano-systems coupled to broad leads[2].

While attempts are being made to connect nonequilibrium physics to equilibrium concepts[11], the nonequilibrium steady state properties of correlated quantum systems continue to present a formidable challenge to our theoretical understanding. The main difficulty is that a rigorous evaluation of the long-time and steady state properties requires an accurate time propagation, starting from some known initial state and reaching all the way to the steady state. When this relaxation occurs quickly, a range of powerful semi-analytical[12–14] and numerical methods[15–25] are applicable. However, dynamics in strongly correlated systems may exhibit a separation of timescales—for example, the spin-relaxation dynamics in the Kondo regime of a quantum dot are orders of magnitude slower than those of the corresponding charge relaxation. Existing theoretical methods are unable to resolve these timescales reliably in the general case (though progress in analytical methods[26–28] can teach us much about generic aspects of the problem).

In this Letter we show that a combination of bold-line diagrammatic Monte Carlo methods[24,29] and the memory-function approach[25] enables us to significantly extend the time regime accessible and can, in some cases, access steady state information within the Kondo regime (though not deep within the strong-coupling regime). The method is numerically exact and provides unbiased error estimates. While the calculations presented here are for the single impurity Anderson model, a minimal model for strong interactions in the presence of baths, the methodology is applicable to any quantum impurity model[30].

The Anderson impurity model is defined by the Hamiltonian

$$H = H_S + H_B + V, \tag{1}$$

where H_S describes the interacting system (or dot) part, H_B the non-interacting bath (or leads) part, and V the system–bath coupling part:

$$H_S = \sum_{i=\uparrow\downarrow} \varepsilon_i d_i^\dagger d_i + U d_\uparrow^\dagger d_\uparrow d_\downarrow^\dagger d_\downarrow, \tag{2}$$

$$H_B = \sum_{k,i=\uparrow\downarrow} \varepsilon_{ik} a_{ik}^\dagger a_{ik}, \tag{3}$$

$$V = \sum_{k,i=\uparrow\downarrow} t_{ik} d_i a_{ik}^\dagger + t_{ik}^* a_{ik} d_i^\dagger. \tag{4}$$

Here $\uparrow$ and $\downarrow$ represent electronic spin, the d_i and $d_i^\dagger$ are fermionic system operators for dot states with energy ε_i, a_{ik} and $a_{ik}^\dagger$ are fermionic lead operators with energy ε_{ik} and the t_{ik} are coupling constants. k is an index iterating over the lead states. The relevant aspect of the ε_{ik} and t_{ik} are encoded in $\Gamma(\varepsilon) \equiv 2\pi \sum_k |t_k|^2 \delta(\varepsilon - \varepsilon_{ik})$.

Refs.[31–33] have shown that the reduced density matrix $\sigma(t) = \mathrm{Tr}_B\{\rho(t)\}$ ($\rho(t)$ being the full density matrix and $\mathrm{Tr}_B\{...\}$ denoting a trace over all bath degrees of freedom) of any system of the form of Eq. (1) exactly obeys the Nakajima–Zwanzig–Mori equation

$$i\hbar \frac{\mathrm{d}\sigma(t)}{\mathrm{d}t} = \mathcal{L}_{H_S}\sigma(t) + \vartheta(t) - \frac{i}{\hbar}\int_0^t \mathrm{d}\tau\, \kappa(\tau)\, \sigma(t-\tau). \tag{5}$$

Here, the Liouvillian superoperator $\mathcal{L}_{H_S} A \equiv [H_S, A]$ denotes a commutation with the system Hamiltonian H_S, with the same notation defining $\mathcal{L}_V$ and $\mathcal{L}_H$; $\vartheta(t)$ is an

initial correlation term which vanishes for factorized initial conditions $\rho(0) \equiv \rho_B \otimes \sigma(0)$; and ρ_B is the initial bath density matrix. κ is known as the memory kernel and may be obtained by solving[34]

$$\kappa(t) = i\hbar\dot{\Phi}(t) - \Phi(t)\mathcal{L}_S + \frac{i}{\hbar}\int_0^t \mathrm{d}\tau \Phi(t-\tau)\kappa(\tau), \quad (6)$$

where the superoperator $\Phi(t) \equiv \mathrm{Tr}_B\left\{\mathcal{L}_V e^{-\frac{i}{\hbar}\mathcal{L}_H t}\rho_B\right\}$ must in general be obtained from a many body computation whose expense rapidly increases as t increases. Evaluation of $\Phi(t)$ for t up to a cutoff time t_c allows an exact evaluation of $\kappa(t < t_c)$. Setting $\kappa(t > t_c) = 0$ defines the cutoff approximation, whose convergence may be monitored from the dependence of results on t_c as t_c is increased. In the case of the Anderson impurity model, Ref.[25] has shown that if one is only interested in evaluating the diagonal elements of the density matrix, all the supermatrix elements $\Phi_{ij,qq'} \equiv (|i\rangle\langle j|)^\dagger \Phi |q\rangle\langle q'|$ of Φ having $i \neq j$ or $q \neq q'$ can be set to zero, with the remaining elements determined by:

$$\begin{aligned}\Phi_{ii,qq} = {} & \delta_{i0}\left(\varphi^{(1)}_{qq} + \varphi^{(3)}_{qq}\right) + \delta_{i1}\left(\varphi^{(2)}_{qq} - \varphi^{(3)}_{qq}\right) \\ & + \delta_{i2}\left(-\varphi^{(1)}_{qq} + \varphi^{(4)}_{qq}\right) + \delta_{i3}\left(-\varphi^{(2)}_{qq} - \varphi^{(4)}_{qq}\right), \quad (7)\end{aligned}$$

$$\varphi^{(m)}_{qq}(t) = 2i\Im\sum_k \mathrm{Tr}_B\left\{\rho_B\langle q|A^{(m)}_k(t)|q\rangle\right\}, \quad (8)$$

where $A^{(1)}_k = t_{\uparrow k}d_\uparrow d_\downarrow d^\dagger_\downarrow a^\dagger_{\uparrow k}$, $A^{(2)}_k = t_{\uparrow k}d_\uparrow d^\dagger_\downarrow d_\downarrow a^\dagger_{\uparrow k}$, $A^{(3)}_k = t_{\downarrow k}d_\uparrow d^\dagger_\uparrow d_\downarrow a^\dagger_{\downarrow k}$ and $A^{(4)}_k = t_{\downarrow k}d^\dagger_\uparrow d_\uparrow d_\downarrow a^\dagger_{\downarrow k}$.

The evaluation of the $\varphi^{(m)}_{qq}(t)$ has previously been performed with real time path integral Monte Carlo (RT-PIMC) methods[15,25,35], revealing that, in the presence of strong electronic correlations, the memory kernel may develop long tails. Near the Kondo regime this effect becomes particularly pronounced, making it impossible to converge the cutoff approximation and highlighting the need for methods able to obtain κ for longer times. Here we show that the problem can to a large extent be solved by using the bold expansion for impurity models[29], a technique related to bold-line methods for lattice systems[36–38]. The bold expansion is based on a stochastic Monte Carlo sampling of diagrammatic corrections to the propagators obtained from an infinite partial summation, rather than a sampling of all diagrams. Intrinsic to the method is a tradeoff between complexity and memory requirements of the initial partial resummation and the number of additional diagrams which must be stochastically evaluated. The resulting procedure converges at lower expansion order and greatly reduces the severity of the dynamic sign problem, in practice more than doubling the accessible time scales relative to a bare expansion and allowing reliable estimates of the memory kernel down to much lower temperatures. This allows access to dynamics exhibiting arbitrarily long timescales at those temperatures.

In the nonequilibrium case, diagrams must be evaluated on the Keldysh contour. We find it advantageous to employ a "BoldOCA" built on the one-crossing approximation (OCA)[29,39]. Fig. 1 illustrates this in diagrammatic terms: the bold-line propagators and vertex functions (which allow for the summation over hybridization lines connecting pairs of times on the two different halves of the Keldysh contour) are obtained from the solution of the OCA equations, and used in an expansion which samples diagrams of all crossing orders. The increase in complexity and memory required to obtain the initial OCA solution (not needed in the bare expansion) is more than compensated for by the reduction in the number of diagrams which must be stochastically sampled. Unbiased error estimates are obtained by jackknife analysis on data from multiple, uncorrelated Monte Carlo runs (typically 5–10).

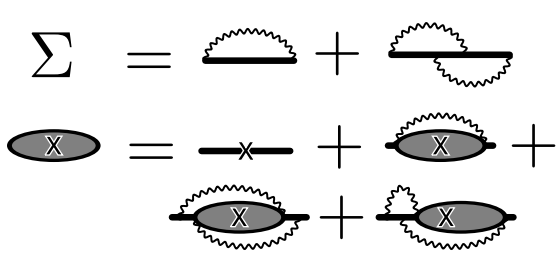

Figure 1. Self energies and vertex equations used within the OCA based bold expansion. Solid lines represent bare propagators, bold lines are dressed propagators, wavy lines are hybridization interactions and shaded regions are vertex functions. The vertices are defined on the unfolded Keldysh contour, such that the final time on the contour is marked by the central "X" and both edges of the contour stand for the initial time.

We assume a wide, flat band $\Gamma_i(E) = \Gamma^L_i(E) + \Gamma^R_i(E)$ with $\Gamma^{L(R)}_i(E) = \frac{\Gamma/2}{\left(1+e^{\nu(E-\varepsilon_c)}\right)\left(1+e^{-\nu(E+\varepsilon_c)}\right)}$; here ε_c and ν are the band cutoff energy and its inverse cutoff width, and L and R are respectively left and right lead indices. We restrict our calculations to the symmetric Anderson impurity model. We apply a magnetic field h in order to generate a non-zero magnetization, setting $\varepsilon_i = -\frac{U}{2} \pm \frac{h}{2}$ (the formalism is more general and does not rely on this symmetry). We choose Γ as our energy unit, and throughout the rest of this paper set $U = 5\Gamma$, $\varepsilon_c = 10\Gamma$ and $\Gamma\nu = 10$. The initial conditions are determined by assuming an initially decoupled system, having left and right leads thermally equilibrated at a temperature β and chemical potentials $\mu_L = \frac{V}{2}$ and $\mu_R = -\frac{V}{2}$, respectively. This defines the lesser and greater hybridization functions $\Delta^<_{L(R)}(\omega) = -if_{L(R)}(\omega)\Gamma_{L(R)}(\omega)$ and $\Delta^>(\omega) = i\left(1 - f_{L(R)}(\omega)\right)\Gamma_{L(R)}(\omega)$, which depend on the temperature and chemical potentials through the Fermi occupation function $f_{L(R)}(\omega) = \frac{1}{1+e^{\beta\left(\omega-\mu_{L(R)}\right)}}$. At these parameters, the Kondo temperature is given by $\Gamma\beta_K \equiv \frac{\Gamma}{T_K} \simeq 3.4$[40].

At zero voltage the method can be benchmarked against the equilibrium magnetization[29,41,42]. The top

left panel of Fig. 2 displays the steady state magnetization predicted by the proposed method at $V = 0$, plotted against the inverse cutoff time $\frac{1}{\Gamma t_c}$ at several temperatures. For the very small magnetic field $h = 0.01\Gamma$ in Fig. 2, the relative errors are rather large, but considered on the full scale of the magnetization the precision demonstrated here is remarkable. Lower temperatures exacerbate the sign problem, resulting in larger errors and longer computation times.

The effects of taking the system out of equilibrium are illustrated in the lower left panel of Fig. 2. Here a constant temperature $\beta\Gamma = 1$ is maintained while the bias voltage V is varied at $h = 0.1\Gamma$; the numerically exact $V = 0$ result is also shown. This plot clearly illustrates that convergence of the method generally occurs at even shorter times in nonequilibrium conditions—consistent with expectations, equilibrium exhibits the longest memory while at larger voltages the plateau is reached at shorter cutoff times.

An independent approach to verifying convergence relies on direct examination of individual elements of the memory kernel as a function of time. Several representative elements are displayed at $h = 0.01\Gamma$ and $\beta\Gamma = 1$ in the top right panel of Fig. 2, with the inset highlighting short times. Within the times accessible by BoldOCA, the memory kernel elements go to zero within the numerical accuracy. Below this, on the same time scale and for the same parameters, the time dependence of the three distinct elements of the reduced density matrix σ is plotted for an initially magnetized dot in the lower right panel of Fig. 2. With this initial condition and within the symmetric Anderson impurity model, the diagonal density matrix entries σ_0 and σ_3, which express charging dynamics, are identical. They both relax so rapidly that their steady state values could have been obtained to very good accuracy without recourse to memory techniques. The difference in scale between the spin relaxation time of σ_1, σ_2 and the memory decay in the upper panel, however, is striking—and is why our memory kernel methods are essential for obtaining long-time behavior. To obtain a reasonable converged steady state directly, one would need to reach times $\Gamma t \gtrsim 20$ with errors of similar magnitude compared to what we have obtained at $\Gamma t = 2$ with the current approach. The exponential scaling in time typical of all general exact methods makes this unfeasible.

We now turn to the presentation of results. The left panels of Fig. 3 show the time evolution of the magnetization from an initially polarized state at different voltages and magnetic fields, with $\beta\Gamma = 1$. At low voltages two separate relaxation timescales are apparent: immediate fast relaxation followed by later slow relaxation. At high enough fields (bottom), an overshoot effect appears along with oscillatory behavior which is seen more clearly in the upper right panel. As we increase the voltage the second timescale is suppressed and eventually the relaxation becomes exponential. However, the voltage required in order to reach this regime is surprisingly large. In the top

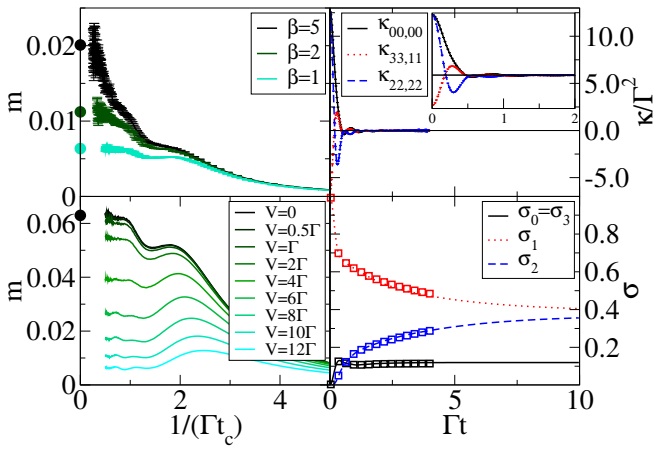

Figure 2. Top left panel: The steady-state magnetization obtained from the memory formalism at several temperatures plotted as a function of the inverse cutoff time, and compared in the equilibrium cases to exact CT-QMC results shown as circles, for $h = 0.01\Gamma$ and $V = 0$. Bottom left panel: The same plot at $\beta\Gamma = 1$ and $h = 0.1\Gamma$, for several voltages. Right panels: equilibrium memory kernel κ (top) and populations σ_i (bottom) as a function of time for $\beta\Gamma = 1$ and $h = 0.01\Gamma$. The inset shows the memory kernel at short times. The squares in the bottom right panel are approximate OCA results.

right panel of Fig. 3, we show that nonequilibrium OCA and the simpler one-crossing approximation or NCA (neither supplemented by QMC) are poor approximation for $h \neq 0$, in contrast to the approach introduced here.

In the lower right panel of Fig. 3, we show an example of the temperature dependence of the $t \to \infty$ limit of the magnetization at constant magnetic field and a range of bias voltages. Interestingly, at higher voltages (but substantially below $\frac{V}{2} \approx \varepsilon_c$ where the lead chemical potentials approach the band cutoff) the temperature dependence becomes non-monotonic. We believe this is a population switching effect[43], which leads to a suppression of the magnetization by population transfer from the magnetized $|1\rangle$ and $|2\rangle$ states to the unmagnetized $|0\rangle$ and $|3\rangle$ states which are activated for $V \gtrsim U$. The rate for this transfer process is approximately proportional to the lead occupation at the energy difference between the states: $f(\beta, \Delta E, \mu) = \frac{1}{1+e^{\beta(\Delta E - \mu)}}$, with ΔE equal to half the interaction energy $\frac{U}{2}$ and $\mu = \frac{V}{2}$ or $-\frac{V}{2}$, depending on the lead. f is therefore an increasing function of temperature for $V < U$ and a decreasing one for $V > U$. At small voltages the effect of the population transfer results in a reduction of the magnetization (as expected), while at large voltages the population transfer enhances the intermediate-temperature magnetization. At still larger temperatures, the nonequilibrium effects are washed away and normal thermal suppression of the magnetization occurs.

In Fig. 4 we display the steady state voltage depen-

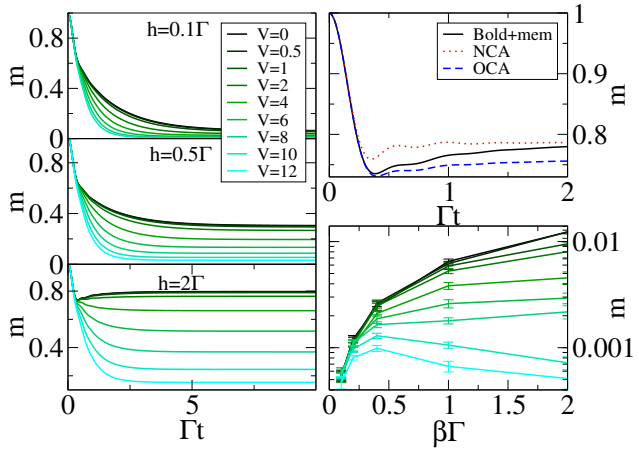

Figure 3. Left panels: Time dependence of the cutoff-converged magnetization at $\beta\Gamma = 1$ starting from a fully magnetized dot, at different magnetic fields h and bias voltages V. Top right: Comparison with NCA and OCA at $h = 2\Gamma$ and $V = 0$. Bottom right: Temperature dependence of the $h = 0.01\Gamma$ steady state magnetization at different voltages.

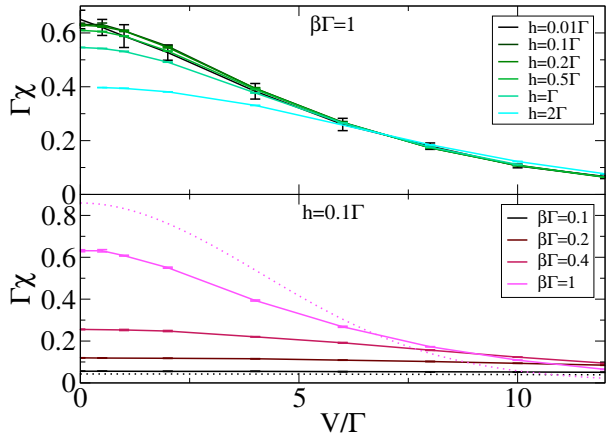

Figure 4. Generalized magnetic susceptibility $\chi \equiv \frac{m}{h}$ as a function of voltage, for (top) different magnetic fields and (bottom) different temperatures, at $h = 0.1\Gamma$. Approximate results from a master equation calculation are shown in dotted lines for the lowest and highest temperatures in the lower panel.

dence of the generalized magnetic susceptibility $\chi \equiv \frac{m}{h}$. At small h this quantity is h-independent. The top panel shows clearly how the regime in which m is linear in h depends on voltage at a constant temperature. The bottom panel of Fig. 4 shows the voltage dependence at different temperatures within the linear regime. One immediately noticeable feature is the decrease of χ with increasing β at high voltage, which corresponds to the non-monotonic temperature dependence discussed in the bottom panel of Fig. 4. A second interesting feature is the fact that the plots have a simple, Lorentzian-like structure, suggesting that the results may be in a regime accessible to analytical methods based on performing logarithmic corrections around rate equations[44]: in the dotted lines in the bottom panel we show for comparison results obtained by solving the classical rate equations (obtained by simple perturbation theory to second order in the hybridization). The large discrepancy between the master equation and numerically exact results at $\beta\Gamma = 1$, demonstrating the need for methods such as those introduced here.

In conclusion, by unifying numerically exact bold Monte Carlo methods with the exact memory approach we have developed a new, numerically exact formalism free from systematic errors and well suited for the real time solution of nonequilibrium quantum impurity models. In practice, the capabilities of this formalism are unparalleled: the method generates precise, converged results at all timescales, in cases where the current state-of-the-art approximate methods clearly fail. For the nonequilibrium Anderson impurity model, the formalism performs well even as one enters the Kondo regime, a regime previously inaccessible with accurate numerical methods. It should however be noted that the computational difficulty increases at low temperatures; in the strong coupling regime T_K becomes very small, eventually dropping below our accessible temperature range (though at the absolute temperature used in this work strong coupling remains accessible).

Our formalism has allowed us to explore the detailed behavior of the nonequilibrium magnetization, and we have made predictions regarding multi-scale, oscillatory quenching dynamics at high magnetic fields; the effect of voltage on dynamical relaxation; and population-driven reversal of the magnetization's temperature dependence at high voltages. These results are obtained at parameters where no other currently available method is reliable. As the temperature is further lowered, one expects to encounter the formation of Kondo peaks at the chemical potential. How this will affect the behavior described here remains an interesting and open question, and work is currently being carried out to further investigate this issue. Future research will address lower temperatures and a wider variety of observables; it is also worth stressing that both bold techniques and the memory formalism are not specific to the Anderson impurity model, and are expected to have many more applications.

ACKNOWLEDGMENTS

GC is grateful to the Azrieli Foundation for the award of an Azrieli Fellowship and to the Yad Hanadiv–Rothschild Foundation for the award of a Rothschild Postdoctoral Fellowship and acknowledges the hospitality of MPI PKS Dresden and Columbia University. This

work was supported by the US–Israel Binational Science Foundation and by the FP7 Marie Curie IOF project HJSC. DRR acknowledges NSF CHE-1213247. AJM acknowledges NSF DMR 1006282. Our implementations were based on the ALPS[45] libraries.

[1] D. Goldhaber-Gordon, H. Shtrikman, D. Mahalu, D. Abusch-Magder, U. Meirav, and M. A. Kastner, Nature **391**, 156 (1998).
[2] R. Hanson, L. P. Kouwenhoven, J. R. Petta, S. Tarucha, and L. M. K. Vandersypen, Rev. Mod. Phys. **79**, 1217 (2007).
[3] J. Park, A. N. Pasupathy, J. I. Goldsmith, C. Chang, Y. Yaish, J. R. Petta, M. Rinkoski, J. P. Sethna, H. D. Abruna, P. L. McEuen, and D. C. Ralph, Nature **417**, 722 (2002).
[4] J. R. Heath and M. A. Ratner, Phys. Today **56**, 43 (2003).
[5] J.-P. Brantut, J. Meineke, D. Stadler, S. Krinner, and T. Esslinger, Science **337**, 1069 (2012).
[6] P. W. Anderson, Phys. Rev. **124**, 41 (1961).
[7] R. Brako and D. M. Newns, J. Phys. C Solid State **14**, 3065 (1981).
[8] A. Georges, G. Kotliar, W. Krauth, and M. J. Rozenberg, Rev. Mod. Phys. **68**, 13 (1996).
[9] Y. Meir, N. S. Wingreen, and P. A. Lee, Phys. Rev. Lett. **70**, 2601 (1993).
[10] A. Rosch, J. Kroha, and P. Wölfle, Phys. Rev. Lett. **87**, 156802 (2001).
[11] P. Dutt, J. Koch, J. E. Han, and K. L. Hur, arXiv:1101.1526 (2011), ann. Phys. 326 2963-2999 (2011).
[12] D. C. Langreth and P. Nordlander, Phys. Rev. B **43**, 2541 (1991).
[13] T. Fujii and K. Ueda, Phys. Rev. B **68**, 155310 (2003).
[14] M. Eckstein, M. Kollar, and P. Werner, Phys. Rev. Lett. **103**, 056403 (2009).
[15] L. Mühlbacher and E. Rabani, Phys. Rev. Lett. **100**, 176403 (2008).
[16] R. Bulla, T. A. Costi, and T. Pruschke, Rev. Mod. Phys. **80**, 395 (2008).
[17] F. B. Anders, J. Phys. Cond. Mat. **20**, 195216 (2008).
[18] S. Weiss, J. Eckel, M. Thorwart, and R. Egger, Phys. Rev. B **77**, 195316 (2008).
[19] P. Werner, T. Oka, and A. J. Millis, Phys. Rev. B **79**, 035320 (2009).
[20] M. Schiró and M. Fabrizio, Phys. Rev. B **79**, 153302 (2009).
[21] F. Heidrich-Meisner, A. E. Feiguin, and E. Dagotto, Phys. Rev. B **79**, 235336 (2009).
[22] H. Wang and M. Thoss, The Journal of chemical physics **131**, 024114 (2009).
[23] D. Segal, A. J. Millis, and D. R. Reichman, Phys. Rev. B **82**, 205323 (2010).
[24] E. Gull, D. R. Reichman, and A. J. Millis, Phys. Rev. B **84**, 085134 (2011).
[25] G. Cohen and E. Rabani, Phys. Rev. B **84**, 075150 (2011).
[26] S. G. Jakobs, M. Pletyukhov, and H. Schoeller, Phys. Rev. B **81**, 195109 (2010).
[27] M. Pletyukhov, D. Schuricht, and H. Schoeller, Phys. Rev. Lett. **104**, 106801 (2010).
[28] M. Pletyukhov and H. Schoeller, Phys. Rev. Lett. **108**, 260601 (2012).
[29] E. Gull, D. R. Reichman, and A. J. Millis, Phys. Rev. B **82**, 075109 (2010).
[30] S. S. M. at [URL will be inserted by publisher] for details and background regarding the methodology., .
[31] S. Nakajima, Prog. Theor. Phys. **20**, 948–959 (1958).
[32] R. Zwanzig, J. Chem. Phys. **33**, 1338 (1960).
[33] H. Mori, Prog. Theor. Phys. **33**, 423–455 (1965).
[34] M.-L. Zhang, B. J. Ka, and E. Geva, J. Chem. Phys. **125**, 044106 (2006).
[35] P. Werner, T. Oka, and A. J. Millis, Cond. Mat. , 0810.2345 (2008).
[36] N. Prokof'ev and B. Svistunov, Phys. Rev. Lett. **99**, 250201 (2007).
[37] N. V. Prokof'ev and B. V. Svistunov, Phys. Rev. B **77**, 125101 (2008).
[38] K. Van Houcke, F. Werner, E. Kozik, N. Prokof'ev, B. Svistunov, M. J. H. Ku, A. T. Sommer, L. W. Cheuk, A. Schirotzek, and M. W. Zwierlein, Nat Phys **8**, 366 (2012).
[39] T. Pruschke and N. Grewe, Z. Phys. B Cond. Mat. **74**, 439 (1989).
[40] A. C. Hewson, *The Kondo Problem to Heavy Fermions* (Cambridge University Press, Cambridge, 1993).
[41] P. Werner, A. Comanac, L. de' Medici, M. Troyer, and A. J. Millis, Phys. Rev. Lett. **97**, 076405 (2006).
[42] E. Gull, A. J. Millis, A. I. Lichtenstein, A. N. Rubtsov, M. Troyer, and P. Werner, Rev. Mod. Phys. **83**, 349 (2011).
[43] G. Cohen and E. Rabani, Mol. Phys. **106**, 341 (2008).
[44] J. Paaske, A. Rosch, and P. Wölfle, Phys. Rev. B **69**, 155330 (2004).
[45] B. Bauer *et al.*, J. Stat. Mech. Theory E. **2011**, P05001 (2011).